Magnetic resonance imaging (MRI) and dynamic MRI evaluation of extranodal non-Hodgkin lymphoma in oral and maxillofacial regions

Hidenobu Matsuzaki, DDS,[a] Marina Hara, DDS,[b] Yoshinobu Yanagi, DDS,[c] Jun-ichi Asaumi, DDS, DMSci,[d] Naoki Katase, DDS, PhD,[e] Teruhisa Unetsubo, DDS, PhD,[b] Miki Hisatomi, DDS, PhD,[f] Hironobu Konouchi, DDS, PhD,[c] Toshihiko Takenobu, DDS, PhD,[b] and Hitoshi Nagatsuka, DDS, PhD,[g]
Okayama, Japan
OKAYAMA UNIVERSITY

Objective. The purpose of this study was to evaluate the diagnostic value of magnetic resonance imaging (MRI), especially dynamic contrast-enhanced magnetic resonance imaging (DCE-MRI), in extranodal non-Hodgkin lymphoma (NHL) of oral and maxillofacial regions.
Study design. Thirteen cases with extranodal NHL were examined using MRI. T1-weighted images (T1WI) and T2-weighted images (T2WI) or short TI inversion recovery (STIR) images were obtained in all cases. Contrast-enhanced images and DCE-MRI were acquired in 10 and 7 cases, respectively. On DCE-MRIs, we analyzed the parameters as follows: contrast index at maximal contrast enhancement (CImax), maximum contrast index (CI) gain/CImax ratio, and washout ratios (WR_{300}, WR_{600}, and WR_{900}) at 300, 600, and 900 seconds after contrast medium injection.
Results. The signal intensity of all lesions was hypointense to isointense on T1WIs and showed variable contrast enhancement patterns. On T2WIs and STIR images, the signal intensity was isointense to hyperintense in almost all cases. Analysis of DCE-MRI parameters in extranodal NHLs resulted in the identification of 4 types of CI curves according to CImax and WR: (1) CImax greater than 2.0 and WR_{900} greater than 40%, (2) CImax greater than 2.0 and WR_{900} less than 40%, (3) CImax less than 1.5 and WR_{900} greater than 40%, and (4) CImax less than 1.5 and WR_{900} greater than 40%.
Conclusions. The signal intensities on MRI were not specific to extranodal NHL and resembled those of other tumor types. When CImax was less than 1.5 or WR900 was less than 40%, these parameters contributed to diagnosis in extranodal NHLs.
(Oral Surg Oral Med Oral Pathol Oral Radiol 2012;113:126-133)

Malignant lymphomas are divided into non-Hodgkin and Hodgkin groups, and approximately 40% of non-Hodgkin lymphomas (NHLs) arise at extranodal sites outside the lymphoid system.[1] The most common sites of extranodal NHL in the oral region are the palate and maxilla.[2-7] The common clinical symptom is mass formation with or without ulceration, and the radiological sign of lesions involving the jawbone is diffuse bone resorption, similar to those of periodontal inflammation, osteomyelitis, and other malignant tumors.[3-10] Some authors have reported the existence of various magnetic resonance (MR) findings for extranodal NHL of the head and neck region and nonspecific signal characteristics.[11-15]

It has been reported that the time versus signal-intensity curve, which uses the parameters of dynamic contrast-enhanced magnetic resonance imaging (DCE-MRI), is useful for diagnosis of some lesions.[16-29] Furthermore, using the calculated values from parameters of DCE-MRI, such as the contrast index (CI) curve, might make it possible to investigate the characteristics of lesions and contribute to diagnosis.[15,30-37] We reported that the CI of malignant lymphomas (including nodal lymphomas in the head and neck region) have characteristic values and maximum CI values that are useful for distinguishing malignant lymphomas from oral squamous cell carcinomas.[15,35]

In the present study, we retrospectively evaluated magnetic resonance imaging (MRI) studies of extranodal NHL of oral and maxillofacial regions. Furthermore, we evaluated the diagnostic value of the parameters of CI curves on DCE-MRI.

MATERIAL AND METHODS

Patients

Twenty-six patients were histopathologically diagnosed with extranodal NHL in our hospital between April 1993 and December 2009. Of these patients, we

[a]Assistant Professor, Department of Oral Diagnosis and Dentomaxillofacial Radiology.
[b]Research Fellow, Department of Oral and Maxillofacial Radiology.
[c]Senior Assistant Professor, Department of Oral Diagnosis and Dentomaxillofacial Radiology.
[d]Professor, Department of Oral and Maxillofacial Radiology.
[e]Assistant Professor, Department of Oral Pathology and Medicine.
[f]Assistant Professor, Department of Oral and Maxillofacial Radiology.
[g]Professor, Department of Oral Pathology and Medicine.
Received for publication Apr 2, 2011; returned for revision Jul 19, 2011; accepted for publication Jul 29, 2011.

2212-4403/$ - see front matter
doi:10.1016/j.tripleo.2011.07.038

Table I. Clinical information, tumor size, and MRI findings in 13 patients with malignant lymphoma

						T1WI		*T2WI*		*STIR*		*CE-T1WI*	
Case	*Age*	*Sex*	*Loc*	*Pathology*	*Size on MRI, mm*	*Homogeneity*	*Signal intensity*	*Homogeneity*	*Signal intensity*	*Homogeneity*	*Signal intensity*	*Homogeneity*	*DE*
1	63	F	BM	DLBCL	25 × 10 × 30	Homo	Iso	Nearly homo	Iso-Hyper	—	—	—	—
2*	67	M	Palate	DLBCL	55 × 36 × 22	Homo	Iso	Hetero	Hypo-Iso	—	—	Nearly homo	L
3	74	F	Tongue	DLBCL	16 × 18 × 16	Nearly homo	Hypo-Iso	Homo	Slightly Hyper	—	—	—	—
4*	68	M	BM	MALT	29 × 16 × 41	Homo	Iso	Nearly homo	Iso-Hyper	—	—	Nearly homo	M-H
5*	58	M	UG	DLBCL	38 × 19 × 22	Homo	Iso	Nearly homo	Iso-Hyper	—	—	Nearly homo	M-H
6*	71	M	MaxS	DLBCL	59 × 43 × 49	Homo	Iso	Nearly homo	Hypo-Iso	—	—	Nearly homo	L-M
7†	44	M	UG	ATLL	26 × 32 × 24	Homo	Iso	—	—	Nearly homo	Iso	Nearly homo	M
8*	79	F	Palate	DLBCL	23 × 20 × 10	Homo	Iso	—	—	Nearly homo	Iso	Homo	L
9*	58	F	BM	FL	15 × 7 × 10	Nearly homo	Hypo-Iso	—	—	Nearly homo	Iso-Hyper	Hetero	L
10†	74	F	UG	DLBCL	53 × 50 × 37	Nearly homo	Hypo-Iso	Nearly homo	Iso-Hyper	—	—	Hetero	M-H
11*	68	F	Maxilla	DLBCL	39 × 40 × 32	Homo	Iso	—	—	Hetero	Iso-Hyper	Hetero	L
12†	73	F	Palate	MALT	22 × 21 × 16	Nearly homo	Hypo-Iso		Nearly homo	Iso-Hyper	——	Nearly homo	L
13	68	F	Palate	FL	18 × 12 × 9	Homo	Iso	Nearly homo	Hypo-Iso	—	—	—	—

MRI, magnetic resonance imaging; *Loc,* location; *WI,* weighted image; *CE,* contrast-enhanced; *DE,* degree of enhancement by contrast medium; *BM,* buccal mucosa; *UG,* upper gingiva; *MaxS,* maxillary sinus; *DLBCL,* diffuse large B-cell lymphoma; *MALT,* mucosa-associated lymphoid tissue; *ATLL,* adult T-cell leukemia/lymphoma; *FL,* follicular lymphoma; *Homo,* homogenous; *Hetero,* heterogeneous; H*ypo,* hypointense; *Iso,* isointense; *Hyper,* hyperintense; *L,* low; *M,* moderate; *H,* high; —, not performed.

*Cases that underwent dynamic contrast-enhanced MRI.

†Cases with contrast enhancement.

evaluated the records of 13 who underwent MR examination with or without contrast medium enhancement in this retrospective study. This study was approved by our institutional review board (No. 232). The patients were 5 men and 8 women with a mean age of 66.5 years (age range, 44-79 years) (Table I).

MRI study protocol

The MR examination was performed using a 1.5-T unit with a head or head-neck coil. T1-weighted images (T1WI) were acquired with a spin-echo sequence using parameters of 500 to 660/15 ms (repetition time/echo time [TR/TE]). T2-weighted images (T2WI) with fat suppression, for 9 cases, or short TI inversion recovery (STIR) images, for 4 cases, were acquired with a turbo–spin-echo sequence, using parameters of 2800 to 3000/90 to 105 ms (TR/TE) for T2WIs and 4500, 6100/60/140 ms (TR/TE/inversion time [TI]) for STIR images. Patient images were taken in both the axial and coronal planes.

In 10 patients, contrast-enhanced T1WIs (CE-T1WIs) with fat suppression were acquired using the same parameters as the unenhanced T1WIs after the administration of contrast medium. In this study, we used 2 types of contrast medium, gadopentetate dimeglumine (Gd-DTPA) and gadodiamide hydrate (Gd-DTPA-BMA). For 7 of these 10 patients, we performed dynamic contrast-enhanced MRI (DCE-MRI) with the conditions described as follows.

The first series of DCE-MRIs was acquired using 3-dimensional fast imaging with a steady-state precession sequence using the following parameters: TR 5 ms; TE 2 ms; flip angle 25°; 16 partitions for a 48-mm slab resulting in an effective thickness of 3 mm; and a 250 × 188-mm rectangular field of view and 256 × 192 matrix resulting in a 0.98 × 0.98-mm pixel size. The first series of DCE-MRI was composed of 21 consecutive scans (17, 14, and 12 consecutive scans for 3 cases, respectively) at 1-second intervals (the acquisition time for each scan was 14 seconds). Total scan time of this series was 180 to 315 seconds. Before the second scan, 0.2 mL/kg contrast medium was administered intravenously for 6 seconds at a rate of approximately 2.0 mL per second with manual injection. CE-T1WIs were acquired after the acquisition of the first series of DCE-MRIs in these 7 patients. In another 3 patients without DCE-MRIs, CE-T1WIs were acquired immediately after administration of the contrast medium.

Second and third series of DCE-MRIs were acquired at approximately 600 to 800 seconds and 900 to 1200 seconds (only at 800 seconds for 1 case) after the administration of contrast medium. Two consecutive scans were applied for the second and third series of DCE-MRIs, resulting in a total scan time of 30 seconds.

Evaluation of MR images

The MR images in 13 cases were retrospectively evaluated for tumor size and signal characteristics. Regarding the signal intensity (SI), the signal from the musculature was interpreted as isointense on T1WI, and the signal from the cerebrospinal fluid was interpreted as hyperintense on T2WI and STIR images. In 9 cases

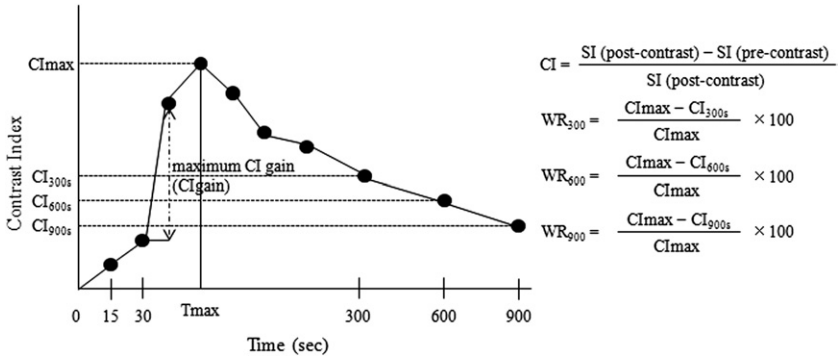

Figure 1. CI curves constructed with DCE-MRI (*left*) and CI curve parameter definitions (*right*). The CI-gain was considered to indicate the maximum gradient on the upslope phase of the enhancement curve, as the CI-gain indicates the difference in the CI between 2 consecutive images. The WR_{300}, WR_{600}, and WR_{900}, expressed as percentage, was defined as follows: CImax – $CI_{300s,\ 600s,\ 900s}$/CImax × 100(%), where CI_{300s}, CI_{600s}, or CI_{900s} is the CI at 300, 600, or 900 seconds after contrast medium administration.

with CE-T1WI, we evaluated the degree of contrast medium enhancement as low to high.

Analysis of DCE-MRI parameters

In 7 cases with DCE-MRIs, we created CI curves using dynamic images to evaluate the flow pattern of contrast medium into the tumor mass. The region of interest (ROI) was drawn to include the maximal region of the tumor mass using the cursor on the monitor. The mean SI on the ROI of each lesion was calculated using a workstation (Synapse Vincent, Fujifilm, Medical Co., Tokyo, Japan). The CI was calculated using the formula CI = (SI [postcontrast] – SI [precontrast])/SI (precontrast). The CI was plotted on a time course to obtain the CI curves. We evaluated the maximum CI gain (CI-gain), the maximum CI (CImax), and the CIgain/CImax ratio for the DCE-MRI parameters. The CIgain was considered to indicate the maximum gradient on the upslope phase of the enhancement curve as CIgain indicates the difference in the CI between 2 consecutive images. The CImax was considered to represent the maximum amplitude of enhancement. The washout ratio (WR_{300}, WR_{600}, and WR_{900}), expressed as a percentage, was defined as follows: CImax – $CI_{300s,\ 600s,\ 900s}$/CImax × 100(%), where CI_{300s}, CI_{600s}, and CI_{900s} represent the CIs at 300, 600, and 1200 seconds after the administration of contrast medium, respectively. CI_{300s}, CI_{600s}, and CI_{900s} were calculated by obtained or linearly interpolated SIs at 315, 615, and 1215 seconds. The calculation with the linearly interpolated method uses the formula: $y = y_a + (y_b - y_a) / (x_b - x_a) \times (x - x_a)$, where y is the SI to be obtained, x is the time to be obtained, (x, y) is the point to be obtained between point A and point B, point A = (x_a, y_a), and point B = (x_b, y_b); $x_a \leq x \leq x_b$. The parameters of CI curves are summarized in Figure 1.

RESULTS

MR findings (size and characteristics of SI)

The MR findings of all cases are summarized in Table I. The mean greatest dimension of the tumor was 34.2 mm (range: 18-59 mm). On T1WIs, all cases had homogeneous or nearly homogeneous SIs that were hypointense or isointense (Figures 2, *A,* and 3, *A*). On T2WIs (n = 9) and STIR images (n = 4), almost all cases had nearly homogeneous SIs that were isointense or hypointense (Figures 2, *B*, and 3, *B*). On the CE-T1WIs of 10 cases, almost all cases had (nearly) homogeneous SIs, although the degree of enhancement was variable (Figures 2, *C*, and 3, *C*).

DCE-MRI parameters

The CI curves and the DCE-MRI parameters, calculated from a dynamic series, are shown in Figure 4 and Table II. The CI curves of 2 cases, upper gingiva and maxilla, increased rapidly, reaching a CImax of less than 1.2 at 120 to 165 seconds. After that, the CI curves showed a nearly sustained plateau until 600 seconds, and gradually decreased to 1200 seconds. The WR_{300} and WR_{900} values of these cases were less than 20% and 30%, respectively. In the case of the maxillary sinus, the CI curve was similar to those of the upper gingiva and maxilla in the early phase, but showed a greater decrease in the late phase. In this case, the WR_{300} was less than 20%, but the WR_{900} was 48.6%, higher than those of the previous 2 cases. The CIgain of these 3 cases was less than 1.0, and the CIgain/CImax ratio was 40% to 55%.

The CI curves of the other 4 cases (palate, 2; buccal mucosa, 2) increased rapidly, reaching a CImax greater than 2.0 at 30 to 120 seconds. The CIgain of these 4 cases was greater than 1.5, and the

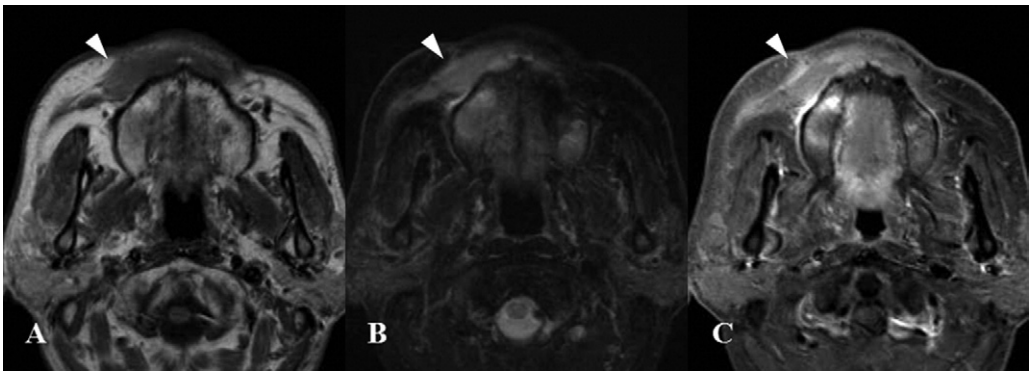

Figure 2. Case 5: A 58-year-old man. **A,** Axial T1WI shows a mass (*arrow*) with nearly homogeneous isointensity at the right upper gingiva (TR/TE = 660/15). **B,** On T2WI, the lesion (*arrow*) appears with nearly homogeneous isointensity to hyperintensity (TR/TE = 3000/90). **C,** On CE-T1WI, the tumor (*arrow*) shows moderate to high homogeneous enhancement.

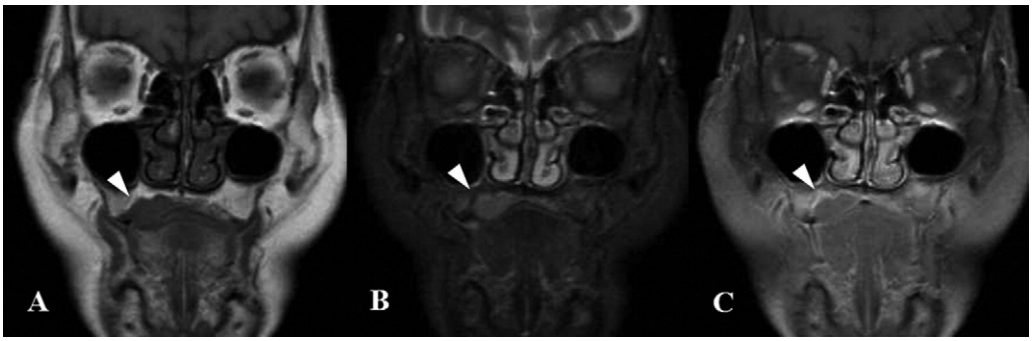

Figure 3. Case 8: A 79-year-old woman. **A,** The mass (*arrow*) of the right hard palate shows homogeneous isointensity on coronal T1WI (TR/TE = 660/15). **B,** The STIR image shows the lesion (*arrow*) with nearly homogeneous isointensity (TR/TE = 4500/60). **C,** On CE-T1WI, there is low homogeneous enhancement in the lesion (*arrow*).

CIgain/CImax ratio was 60% to 85%. In these 4 cases, the WR_{300} was higher than 20%, and the WR_{600} of 3 cases was higher than 40%. In only 1 case of the palate, the WR_{600} and WR_{900} were 29.6% and 35.1%, respectively.

DISCUSSION

Malignant lymphoma is the second most common malignancy in the head and neck region, although its morbidity rate is not high.[38-41] The occurrence rate of extranodal NHL is reported to be approximately 40%, and the most common site in the head and neck region is Waldeyer's ring.[1,8,42-48] Only 3.0% to 9.5% of extranodal NHL arises in the oral region, and its most common sites are the palate and maxilla.[1-7,42,44]

In the cases of extranodal NHL involving the jawbone, the typical radiological finding is diffuse bone resorption, similar to that of periodontal inflammation and other malignant tumors.[3-10] Thus, there is no specific radiological finding for this lesion. Otherwise, when malignant lymphoma arises at the paranasal sinus, computed tomography (CT) images often show specific findings: namely, the tumor permeates the wall without aggressive bony destruction.[11,39,49-52] In NHL of the oral region, such as the jawbone and palate, this finding is not observed as often. Furthermore, in cases arising from soft tissue locally, it is difficult to diagnose NHL by conventional radiographs and CT images.

Generally, the soft tissue contrast resolution of MRI is superior to that of CT; however, MRIs of extranodal lymphoma in the head and neck region have been reported to show variable homogeneity and SI of tumor on both T1WIs and T2WIs.[12-15] The degree of enhancement on CE-T1WIs has been reported to be even more variable; therefore, characterizing this lesion by MRI is difficult. Our results are consistent with previous articles, including our own.[12-15]

Otherwise, in the analysis of DCE-MRI parameters, 2 characteristic patterns of CI curves, relating to the value of CImax and WR, were observed. In the first pattern, extranodal NHLs of the oral region were placed in 2 groups by the value of CImax; one group (n = 4) showed CImax over 2.0, whereas the other (n = 3) showed CImax less than 1.5. The lesions with CImax greater than 2.0 arose from the buccal mucosa or palate;

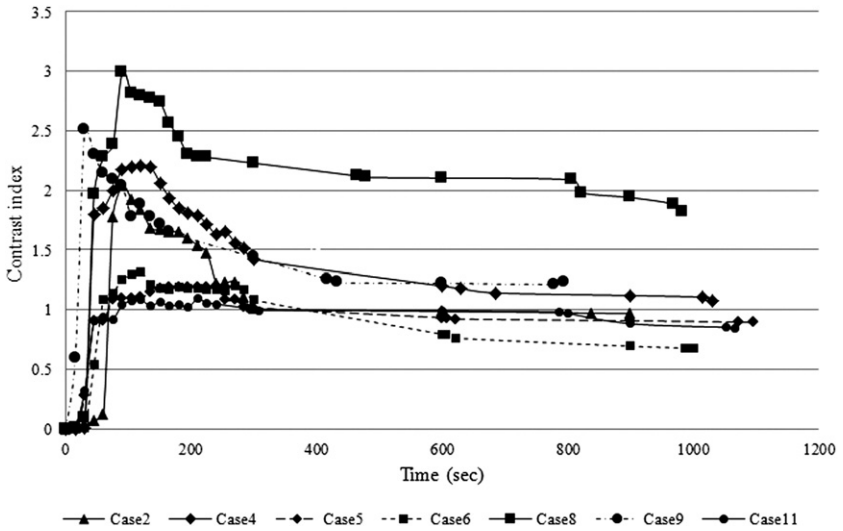

Figure 4. The CI curves of 3 cases (cases 5, 6, and 11) increased rapidly, reaching a CImax less than 1.2 at 120 to 165 seconds. After that, in 2 cases (cases 5 and 11), the CI curves showed a nearly sustained plateau until 600 seconds, and gradually decreased to 1200 seconds. In case 6, the CI curve decreased more sharply than the previous 2 cases in the late phases. The CI curves of the other 4 cases (cases 2, 4, 8, and 9) also increased rapidly, reaching a CImax greater than 2.0 at 30 to 120 seconds. The CI curves in 3 of these cases (cases 2, 4, and 9) showed a gradual decrease until 600 seconds, and then a sustained plateau to 1200 seconds. In case 8, the CI curve continued its gradual decrease to 1200 seconds.

Table II. CImax, $T_{max.}$, CIgain, CIgain/CImax ratio, and $WR_{300\text{-}900}$ in 7 patients

			DCE-MRI						
Case	*Loc*	*Pathology*	*CImax*	$T_{max.}$	*CIgain*	*CIgain/CImax ratio*	WR_{300}	WR_{600}	WR_{900}
2	Palate	DLBCL	2.03	90s	1.66	81.6%	*50.1%	51.2%	52.2%
4	BM	MALT	2.21	120s	1.79	81.0%	*35.7%	45.7%	49.3%
5	UG	DLBCL	1.19	165s	0.63	52.7%	*14.5%	21.5%	23.6%
6	MaxS	DLBCL	1.32	120s	0.55	41.5%	*17.9%	39.7%	47.3%
8	Palate	DLBCL	2.99	90s	1.87	62.6%	25.4%	29.6%	35.1%
9	BM	FL	2.51	30s	1.92	76.6%	42.7%	51.3%	—
11	Maxilla	DLBCL	1.08	120s	0.59	54.5%	7.0%	8.4%	18.1%

CI, contrast index; *DCE-MRI,* dynamic contrast-enhanced magnetic resonance imaging; *WR,* washout ratio; *BM,* buccal mucosa; *DLBCL,* diffuse large B-cell lymphoma; *FL,* follicular lymphoma; *Loc,* location; *MALT,* mucosa-associated lymphoid tissue; *MaxS,* maxillary sinus; *UG,* upper gingiva.

*The cases using measurement value of DCE-MRI to calculate WR.

in contrast, the cases with lower CImax arose from the upper gingiva, maxilla, and maxillary sinus. We previously reported that CImax of NHLs tended to be less than 2.0, a different outcome from that in the present study.[15,35] Our previous articles, however, included 10 nodal lymphoma lesions in 5 patients and 17 lesions in 8 patients overall, and this might have led to the differences in outcome between the past studies and the present study.[15,35] In the previous results for extranodal lymphomas only, the CImax values of 5 lesions were all greater than 2.0 or close to 2.0 and that of another lesion was 1.37. Furthermore, the sites of lesions were the palate (1 case, CImax = 4.24), buccal mucosa (3 cases, CImax = 1.97, 1.93, and 1.37), and orbit (2 cases, CImax = 2.33 and 1.97). The association of lesions with high CImax values with the palate and buccal mucosa is consistent with the findings of the present study.[35] On the other hand, we reported that the CImax of oral squamous cell carcinomas (SCCs) was 2.59 to 2.88, with no relationship between the CImax and the site of lesions.[35-37] The conflicting results of NHL and SCC can be interpreted 2 ways. Focusing on the present study, the degree of enhancement of extranodal NHLs might differ by site, unlike oral SCCs.[35-37] Another interpretation is that the present study might have yielded a lopsided outcome because of the small number of patients.

The second pattern we found related to washout of the contrast medium; extranodal NHLs could be divided into 2 groups by the WR at 900 seconds. The WR_{900} of 1 group (1 palate, 1 buccal mucosa, 1 maxillary sinus) was greater than 40%, with a WR_{600} value greater than 50% in 1 case; this means that CI curves

showed a rapid decrease following a rapid increase. On the other hand, the CI curves of another group (1 upper gingiva, 1 palate, 1 maxilla) showed a gradual decrease, with WR_{900} less than 40%, following a rapid increase. Because there was no correlation between the 2 CImax and WR patterns, our results suggested that extranodal NHLs of the oral region could be divided into at least 4 enhancement types by the CImax and the WR. Especially, we considered that, in the cases with a rapidly decreasing CI curve ($WR_{900} > 40\%$), the degree of enhancement on CE-T1WIs differed from study to study because of the different intervals between contrast medium injection and imaging.[12-15] In 4 cases in this study, we used interpolated values instead of measured values to calculate WR_{600} and WR_{900} using 21 consecutive scans of DCE-MRIs, because no other clinical data were available retrospectively. In the calculation of WRs at each time by the linear interpolation method, we used 2 values anteroposterior to the targeted time. Although the interpolated values might not be accurate, we thought they were reasonable estimates for consideration of the clinical WRs.

We could not evaluate our cases histopathologically because almost all specimens were taken by biopsy, not total extirpation. Several authors reported that DCE-MRI is useful for discrimination between benign and malignant disease, and the enhancement pattern of DCE-MRI has a relationship with tumor angiogenesis.[28,29,36,37,53-56] We also reported that the DCE-MRI parameters of oral SCC, particularly with the CIgain/CImax ratio, were correlated with the microvessel density (MVD) estimated by CD34.[36] This positive correlation in oral SCC means that the more rapidly the CI curve increases, the higher the intratumor MVD of SCC becomes. By mechanically extrapolating the results of oral SCC into extranodal NHLs in this study, the cases with high CIgain/CImax ratios might have higher MVD than the cases with low ratios. Still, the enhancement pattern of both cases with high and low CIgain/CImax ratios showed rapid increase, and the pattern of washout was divided into 2 types: rapidly decreasing and gradually decreasing. Our results suggested that factors other than MVD might affect the enhancement pattern of extranodal NHLs of nonepithelial tumors, unlike that of oral SCCs. We were unable to study the histopathological types of NHLs because the number of patients in our study was too small for such an evaluation. We at least confirmed, however, that the enhancement patterns of diffuse large B-cell lymphoma appeared to be variable.

In conclusion, the SIs on MRI are not specific to extranodal NHL and resemble those for other tumors of the oral and maxillofacial regions. Although the DCE-MRI parameters also lack a characteristic pattern, lesions in which CImax is less than 1.5 or WR_{900} is less than 40% can be identified as extranodal NHLs rather than oral SCCs.

REFERENCES

1. Otter R, Gerrits WB, vd Sandt MM, Hermans J, Willemze R. Primary extranodal and nodal non-Hodgkin's lymphoma. A survey of a population-based registry. Eur J Cancer Clin Oncol 1989;25:1203-10.
2. Eisenbud L, Sciubba J, Mir R, Sachs SA. Oral presentations in non-Hodgkin's lymphoma: a review of thirty-one cases. Part I. Data analysis. Oral Surg Oral Med Oral Pathol 1983;56:151-6.
3. Slootweg PJ, Wittkampf AR, Kluin PM, de Wilde PC, van Unnik JA. Extranodal non-Hodgkin's lymphoma of the oral tissues. An analysis of 20 cases. J Maxillofac Surg 1985;13:85-92.
4. Kemp S, Gallagher G, Kabani S, Noonan V, O'Hara C. Oral non-Hodgkin's lymphoma: review of the literature and World Health Organization classification with reference to 40 cases. Oral Surg Oral Med Oral Pathol Oral Radiol Endod 2008; 105:194-201.
5. van der Waal RI, Huijgens PC, van der Valk P, van der Waal I. Characteristics of 40 primary extranodal non-Hodgkin lymphomas of the oral cavity in perspective of the new WHO classification and the International Prognostic Index. Int J Oral Maxillofac Surg 2005;34:391-5.
6. Söderholm AL, Lindqvist C, Heikinheimo K, Forssell K, Happonen RP. Non-Hodgkin's lymphomas presenting through oral symptoms. Int J Oral Maxillofac Surg 1990;19:131-4.
7. Wolvius EB, van der Valk P, van der Wal JE, van Diest PJ, Huijgens PC, van der Waal I, et al. Primary extranodal non-Hodgkin lymphoma of the oral cavity. An analysis of 34 cases. Eur J Cancer B Oral Oncol 1994;30B:121-5.
8. Epstein JB, Epstein JD, Le ND, Gorsky M. Characteristics of oral and paraoral malignant lymphoma: a population-based review of 361 cases. Oral Surg Oral Med Oral Pathol Oral Radiol Endod 2001;92:519-25.
9. Howell RE, Handlers JP, Abrams AM, Melrose RJ. Extranodal oral lymphoma. Part II. Relationships between clinical features and the Lukes-Collins classification of 34 cases. Oral Surg Oral Med Oral Pathol 1987;64:597-602.
10. Eisenbud L, Sciubba J, Mir R, Sachs SA. Oral presentations in non-Hodgkin's lymphoma: a review of thirty-one cases. Part II. Fourteen cases arising in bone. Oral Surg Oral Med Oral Pathol 1984;57:272-80.
11. Yasumoto M, Taura S, Shibuya H, Honda M. Primary malignant lymphoma of the maxillary sinus: CT and MRI. Neuroradiology 2000;42:285-9.
12. Yasumoto M, Shibuya H, Fukuda H, Takeda M, Mukai T, Korenaga T. Malignant lymphoma of the gingiva: MR evaluation. AJNR Am J Neuroradiol 1998;19:723-7.
13. King AD, Lei KI, Richards PS, Ahuja AT. Non-Hodgkin's lymphoma of the nasopharynx: CT and MR imaging. Clin Radiol 2003;58:621-5.
14. Ueda F, Suzuki M, Matsui O, Minato H, Furukawa M. MR findings of nine cases of palatal tumor. Magn Reson Med Sci 2005;4:61-7.
15. Asaumi J, Yanagi Y, Hisatomi M, Matsuzaki H, Konouchi H, Kishi K. The value of dynamic contrast-enhanced MRI in diagnosis of malignant lymphoma of the head and neck. Eur J Radiol 2003;48:183-7.
16. Hisatomi M, Yanagi Y, Konouchi H, Matsuzaki H, Takenobu T, Unetsubo T, et al. Diagnostic value of dynamic contrast-enhanced MRI for unilocular cystic-type ameloblastomas with homogeneously bright high signal intensity on T2-weighted or STIR MR images. Oral Oncol 2011;47:147-52.

17. Yanagi Y, Asaumi J, Unetsubo T, Ashida M, Takenobu T, Hisatomi M, et al. Usefulness of MRI and dynamic contrast-enhanced MRI for differential diagnosis of simple bone cysts from true cysts in the jaw. Oral Surg Oral Med Oral Pathol Oral Radiol Endod 2010;110:364-9.
18. Zelhof B, Lowry M, Rodrigues G, Kraus S, Turnbull L. Description of magnetic resonance imaging-derived enhancement variables in pathologically confirmed prostate cancer and normal peripheral zone regions. BJU Int 2009;104:621-7.
19. Horsthuis K, Lavini C, Bipat S, Stokkers PC, Stoker J. Perianal Crohn disease: evaluation of dynamic contrast-enhanced MR imaging as an indicator of disease activity. Radiology 2009;251:380-7.
20. Thomassin-Naggara I, Bazot M, Daraï E, Callard P, Thomassin J, Cuenod CA. Epithelial ovarian tumors: value of dynamic contrast-enhanced MR imaging and correlation with tumor angiogenesis. Radiology 2008;248:148-59.
21. Eida S, Ohki M, Sumi M, Yamada T, Nakamura T. MR factor analysis: improved technology for the assessment of 2D dynamic structures of benign and malignant salivary gland tumors. J Magn Reson Imaging 2008;27:1256-62.
22. Bloch BN, Furman-Haran E, Helbich TH, Lenkinski RE, Degani H, Kratzik C, et al. Prostate cancer: accurate determination of extracapsular extension with high-spatial-resolution dynamic contrast-enhanced and T2-weighted MR imaging—initial results. Radiology 2007;245:176-85.
23. Tuncbilek N, Karakas HM, Okten OO. Dynamic magnetic resonance imaging in determining histopathological prognostic factors of invasive breast cancers. Eur J Radiol 2005;53:199-205.
24. Hartmann M, Heiland S, Harting I, Tronnier VM, Sommer C, Ludwig R, et al. Distinguishing of primary cerebral lymphoma from high-grade glioma with perfusion-weighted magnetic resonance imaging. Neurosci Lett 2003;338:119-22.
25. Suenaga S, Indo H, Noikura T. Diagnostic value of dynamic magnetic resonance imaging for salivary gland diseases: a preliminary study. Dentomaxillofac Radiol 2001;30:314-8.
26. Hawighorst H, Knapstein PG, Knopp MV, Weikel W, Brix G, Zuna I, et al. Uterine cervical carcinoma: comparison of standard and pharmacokinetic analysis of time-intensity curves for assessment of tumor angiogenesis and patient survival. Cancer Res 1998;58:3598-602.
27. Park J, Inoue S, Ishizuka Y, Shindo H, Kawanishi M, Kakizaki D, et al. Salivary gland masses: dynamic MR imaging and pathologic correlation. Nippon Igaku Hoshasen Gakkai Zasshi 1997;57:581-5.
28. Tsushima Y, Matsumoto M, Endo K. Parotid and parapharyngeal tumours: tissue characterization with dynamic magnetic resonance imaging. Br J Radiol 1994;67:342-5.
29. Takashima S, Noguchi Y, Okumura T, Aruga H, Kobayashi T. Dynamic MR imaging in the head and neck. Radiology 1993;189:813-21.
30. Asaumi J, Hisatomi M, Yanagi Y, Matsuzaki H, Choi YS, Kawai N, et al. Assessment of ameloblastomas using MRI and dynamic contrast-enhanced MRI. Eur J Radiol 2005;56:25-30.
31. Pickles MD, Manton DJ, Lowry M, Turnbull LW. Prognostic value of pre-treatment DCE-MRI parameters in predicting disease free and overall survival for breast cancer patients undergoing neoadjuvant chemotherapy. Eur J Radiol 2009;71: 498-505.
32. Hisatomi M, Asaumi J, Yanagi Y, Konouchi H, Matsuzaki H, Honda Y, et al. Assessment of pleomorphic adenomas using MRI and dynamic contrast enhanced MRI. Oral Oncol 2003;39:574-9.
33. Rieber A, Nüssle K, Merkle E, Kreienberg R, Tomczak R, Brambs HJ. MR mammography: influence of menstrual cycle on the dynamic contrast enhancement of fibrocystic disease. Eur Radiol 1999;9:1107-12.
34. Hisatomi M, Asaumi J, Yanagi Y, Unetsubo T, Maki Y, Murakami J, et al. Diagnostic value of dynamic contrast-enhanced MRI in the salivary gland tumors. Oral Oncol 2007;43:940-7.
35. Asaumi J, Yanagi Y, Konouchi H, Hisatomi M, Matsuzaki H, Kishi K. Application of dynamic contrast-enhanced MRI to differentiate malignant lymphoma from squamous cell carcinoma in the head and neck. Oral Oncol 2004;40:579-84.
36. Unetsubo T, Konouchi H, Yanagi Y, Murakami J, Fujii M, Matsuzaki H, et al. Dynamic contrast-enhanced magnetic resonance imaging for estimating tumor proliferation and microvessel density of oral squamous cell carcinomas. Oral Oncol 2009;45:621-6.
37. Konouchi H, Asaumi J, Yanagi Y, Shigehara H, Hisatomi M, Matsuzaki H, et al. Evaluation of tumor proliferation using dynamic contrast enhanced-MRI of oral cavity and oropharyngeal squamous cell carcinoma. Oral Oncol 2003;39:290-5.
38. Shindoh M, Takami T, Arisue M, Yamashita T, Saito T, Kohgo T, et al. Comparison between submucosal (extra-nodal) and nodal non-Hodgkin's lymphoma (NHL) in the oral and maxillofacial region. J Oral Pathol Med 1997;26:283-9.
39. DePeña CA, Van Tassel P, Lee YY. Lymphoma of the head and neck. Radiol Clin North Am 1990;28:723-43.
40. Cobleigh MA, Kennedy JL. NonHodgkin's lymphomas of the upper aerodigestive tract and salivary glands. Otolaryngol Clin North Am 1986;19:685-710.
41. Duurkens V, Wagener DJ, van den Broek P, Bogman MJ, Kazem I. [Extranodal non-Hodgkin lymphomas of the head and neck.] Ned Tijdschr Geneeskd 1981;125:989-94. Dutch.
42. Aozasa K, Tsujimoto M, Sakurai M, Honda M, Yamashita K, Hanada M, et al. Non-Hodgkin's lymphomas in Osaka, Japan. Eur J Cancer Clin Oncol 1985;21:487-92.
43. Wong DS, Fuller LM, Butler JJ, Shullenberger CC. Extranodal non-Hodgkin's lymphomas of the head and neck. Am J Roentgenol Radium Ther Nucl Med 1975;123:471-81.
44. Freeman C, Berg JW, Cutler SJ. Occurrence and prognosis of extranodal lymphomas. Cancer 1972;29:252-60.
45. Urquhart A, Berg R. Hodgkin's and non-Hodgkin's lymphoma of the head and neck. Laryngoscope 2001;111:1565-9.
46. Jacobs C, Hoppe RT. Non-Hodgkin's lymphomas of head and neck extranodal sites. Int J Radiat Oncol Biol Phys 1985; 11:357-64.
47. McGurk M, Goepel JR, Hancock BW. Extranodal lymphoma of the head and neck: a review of 49 consecutive cases. Clin Radiol 1985;36:455-8.
48. Etemad-Moghadam S, Tirgary F, Keshavarz S, Alaeddini M. Head and neck non-Hodgkin's lymphoma: a 20-year demographic study of 381 cases. Int J Oral Maxillofac Surg 2010;39:869-72.
49. Kondo M, Hashimoto T, Shiga H, Inuyama Y, Iwata Y, Ohigashi N, et al. Computed tomography of sinonasal non-Hodgkin lymphoma. J Comput Assist Tomogr 1984;8:216-9.
50. Matsumoto S, Shibuya H, Tatera S, Yamazaki E, Suzuki S. Comparison of CT findings in non-Hodgkin lymphoma and squamous cell carcinoma of the maxillary sinus. Acta Radiol 1992;33:523-7.
51. Shlansky-Goldberg RD, Rao VM, Choi HY, March DE, Davis PS. Hodgkin disease of the maxillary sinus. J Comput Assist Tomogr 1988;12:507-9.
52. Yang PJ, Carmody RF, Seeger JF. Computed tomography in hematologic malignancies of paranasal sinuses. J Comput Assist Tomogr 1986;10:1003-5.
53. Tuncbilek N, Karakas HM, Altaner S. Dynamic MRI in indirect estimation of microvessel density, histologic grade, and prognosis in colorectal adenocarcinomas. Abdom Imaging 2004;29:166-72.
54. Reddy DB, Jena A, Venugopal P. Magnetic resonance imaging

(MRI) in evaluation of left atrial masses: an in vitro and in vivo study. J Cardiovasc Surg (Torino) 1994;35:289-94.
55. Hulka CA, Smith BL, Sgroi DC, Tan L, Edmister WB, Semple JP, et al. Benign and malignant breast lesions: differentiation with echo-planar MR imaging. Radiology 1995;197: 33-8.
56. Fobben ES, Rubin CZ, Kalisher L, Dembner AG, Seltzer MH, Santoro EJ. Breast MR imaging with commercially available techniques: radiologic-pathologic correlation. Radiology 1995; 196:143-52.

Reprint requests:

Jun-Ichi Asaumi, DDS, DMSci
Department of Oral and Maxillofacial Radiology
Field of Tumor Biology
Okayama University
Graduate School of Medicine, Dentistry, and Pharmaceutical Sciences
5–1, Shikata-cho, 2-Chome, Okayama-city
Okayama, Japan
asaumi@md.okayama-u.ac.jp